

Functional Consequences of the Open Distal Pocket of Dehaloperoxidase-Hemoglobin Observed by Time-Resolved X-ray Crystallography

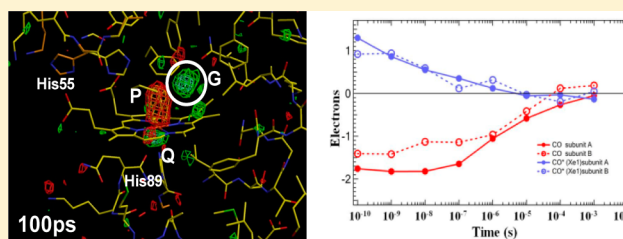
Junjie Zhao,[†] Vukica Srajer,[‡] and Stefan Franzen^{*,†}

[†]Department of Chemistry, North Carolina State University, Raleigh, North Carolina 27695, United States

[‡]Center for Advanced Radiation Sources, The University of Chicago, Chicago, Illinois 60637, United States

S Supporting Information

ABSTRACT: Using time-resolved X-ray crystallography, we contrast a bifunctional dehaloperoxidase-hemoglobin (DHP) with previously studied examples of myoglobin and hemoglobin to understand the functional role of the distal pocket of globins. One key functional difference between DHP and other globins is the requirement that H₂O₂ enter the distal pocket of oxyferrous DHP to displace O₂ from the heme Fe atom and thereby activate the heme for the peroxidase function. The open architecture of DHP permits more than one molecule to simultaneously enter the distal pocket of the protein above the heme to facilitate the unique peroxidase cycle starting from the oxyferrous state. The time-resolved X-ray data show that the distal pocket of DHP lacks a protein valve found in the two other globins that have been studied previously. The photolyzed CO ligand trajectory in DHP does not have a docking site; rather, the CO moves immediately to the Xe-binding site. From there, CO can escape but can also recombine an order of magnitude more rapidly than in other globins. The contrast with DHP dynamics and function more precisely defines the functional role of the multiple conformational states of myoglobin. Taken together with the high reduction potential of DHP, the open distal site helps to explain how a globin can also function as a peroxidase.



Trajectories of diatomic ligands in heme proteins have provided a wealth of information on how such molecules can enter and exit the protein, which must fluctuate to permit their passage. The time-resolved X-ray crystallography technique has provided the most detailed images of the transport of the carbon monoxide ligand (CO) to various cavities within proteins.^{1–5} However, the function of protein cavities is still an open question. Indeed, it is difficult to assign a general function based on the analysis of a single protein because the functional role of cavities may vary from one protein to another. Thus far, two heme proteins, Sperm Whale myoglobin (SWMb)^{2,3} and *Scapharca inaequivalvis* dimeric hemoglobin (HbI),^{4,5} have been the most extensively studied by time-resolved crystallography. Although one is a myoglobin and the other a hemoglobin, they both have the reversible binding of O₂ as their primary function. Despite the rich set of conformational changes associated with the allosteric cooperative transition in photolyzed HbI*CO, the nature of the CO trajectory in this globin has certain similarities with SWMb*CO. (The asterisk indicates a photolyzed carbon monoxide molecule following photon absorption by the heme that leads to rupture of the Fe–CO bond.) Both have a distal docking site, B, where the initially photolyzed CO molecule resides. The B site in both proteins is a distinct ligand-docking site in the distal pocket, not observed is the Xe binding site in either protein.^{2,4} On the basis of experiments designed to block the Xe-binding cavities in SWMb*CO and HbI*CO and on

time-resolved crystallographic studies, it has been deduced that the cavities in these proteins do not constitute an exit route for diatomic ligands.^{6,7} Instead, exit occurs near the distal histidine in both SWMb*CO and HbI*CO. Moreover, previous temperature derivative spectroscopy (TDS) studies show the presence of a nearby docking site and one or more further secondary sites in SWMb^{8–10} and HbI¹¹ where photolyzed CO molecules can reside. Why then does CO migrate to a number of Xe-binding cavities in these proteins after it leaves the B site? This fundamental question has been studied extensively in SWMb using many spectroscopic techniques including TDS and methods such as kinetic hole burning,¹² which makes the connection between the conformation-dependent energy of recombination and the spectroscopic energy of a heme charge transfer band. In this study, we propose that in order to understand the possible function of the cavities in various heme proteins it is necessary to compare a protein with a significant difference in function. We conclude that ligand dynamics studied by time-resolved X-ray crystallography and the protein cavity in DHP identified by a Xe-binding site¹³ are consistent with an open architecture in the distal pocket of the bifunctional hemoglobin, DHP, which explains how it can

Received: August 15, 2013

Revised: October 10, 2013

Published: October 11, 2013



carry out multiple functions. These features distinguish DHP from the more specialized oxygen-transport proteins SWMb and HbI.

Dehaloperoxidase-hemoglobin (DHP), first isolated from the terebellid polychaete *Amphitrite ornata*, is a bifunctional protein that displays significant peroxidase activity under physiological conditions while also having a globin fold and an associated oxygen-transport function.¹⁴ As a hemoglobin, DHP can reversibly bind with O₂, and as a peroxidase, DHP can oxidize 2,4,6-trihalophenol into the corresponding 2,6-dihaloquinone in the presence of H₂O₂. However, normal peroxidase function inactivates the ability of DHP to bind oxygen, leading to a paradox because of the failure of the DHP hemoglobin function.¹⁵ Recently, this functional paradox of DHP has been resolved by establishing that oxyferrous DHP can serve as the resting state of the peroxidase reaction cycle.^{16,17} For a typical peroxidase (e.g., horseradish peroxidase and cytochrome c peroxidase), the ferric state of the heme Fe is the resting state. Thus, DHP appears to have a new type of peroxidase cycle, a ferrous peroxidase cycle.¹⁵ Although it has high peroxidase activity, the oxyferrous peroxidase cycle and unique internal binding sites possessed by DHP distinguish it from other heme peroxidases.^{18,19} The replacement of O₂ bound to the heme Fe by H₂O₂ required by the ferrous peroxidase mechanism suggests that DHP must simultaneously accommodate both O₂ and H₂O₂ in the distal pocket to function. This requirement is quite different from other well-studied hemoglobins and myoglobins. For example, SWMb, which is by far the best studied protein, cannot simultaneously accommodate both CO and H₂O in the distal pocket.^{20–22} The reasons for this may become clearer in comparison with the bifunctional protein, DHP, which has a different requirement for the function of the distal pocket, namely, entry of multiple molecules both for activation and for inhibition of enzymatic function. To address the dynamics of diatomic ligands in DHP, we have conducted a time-resolved X-ray crystallography study of the trajectory of photolyzed carbon monoxide in DHP*CO. The time-dependent structures reveal a qualitatively different CO trajectory than those observed previously in SWMb*CO and HbI*CO.

MATERIALS AND METHODS

Sample Preparation. Ferric DHP A solution was first reduced by a 20-fold excess of sodium dithionite, and DHP-CO complex crystals (space group *P2₁2₁2₁* with unit cell size *a* = 58.90 Å, *b* = 68.59 Å, *c* = 69.35 Å) were then grown by the hanging-drop vapor-diffusion method from 0.2 M ammonium sulfate and 29% poly(ethylene glycol) 8000 at 277 K in 1 atm CO atmosphere. The starting protein concentration was 8 mg mL⁻¹ in 20 mM Na cacodylate pH 6.5 buffer. The crystals were transferred and mounted in 1.0 mm quartz capillaries quickly. A drop of stabilizing solution with saturated sodium dithionite was added into the capillaries to remove excess O₂ before the capillaries were sealed.

Time-Resolved Data Collection. Time-resolved Laue X-ray diffraction experiments were conducted at BioCARS beamline 14ID at the Advanced Photon Source²³ at room temperature by using the pump–probe technique.³ For reaction initiation, we used 480 nm laser pulses from a Spectra-Physics Spitfire Pro picosecond laser coupled to a TOPAS optical parametric amplifier. The laser pulse duration was 35 ps (full width at half-maximum). The laser beam size at the sample was 110 × 550 μm² and laser pulse energy density was 2.7 mJ/mm². The reaction was probed by a single

polychromatic and delayed X-ray pulse of 100 ps in duration. The X-ray beam size was 90 (horizontal) × 70 μm² (vertical) (full width half-maximum). Laser and X-ray beams were perpendicular to each other as described in Figure 1 of Graber et al.²³ Given the limited laser penetration depth because of the high optical density of the crystal, for each crystal orientation, X-ray pulses probed only a 70 μm deep layer of the crystal on the laser-illuminated side of the crystal. For such positioning of the crystal in the X-ray beam, for each crystal orientation, a crystal edge was scanned through the X-ray beam, and the resulting X-ray diffraction was used to guide the crystal positioning. At a fixed angular setting of the crystal, a time series of X-ray diffraction images was recorded using the same crystal volume. The time series consisted of a dark image (laser off) and images at laser X-ray time delays of 100 ps, 1 ns, 10 ns, 1 μs, 10 μs, and 1 ms. The zero time delay refers to the overlap of the leading edges of the pump, laser pulse and the probe, and X-ray pulse. Pump–probe exposure (or just probe in the laser-off case) was repeated five times prior to the detector readout to improve the signal-to-noise ratio of the recorded diffraction patterns. The wait time between consecutive laser pulses was 0.3 s to permit the complete dark-state recovery between the laser pulses and to facilitate heat dissipation. Before collecting a time series for the next angular setting of the crystal, the crystal was translated slightly to expose a partially fresh crystal volume to the X-ray beam, thus minimizing radiation damage. This was repeated for 42 crystal orientations, with a 3° increment between angular settings of the crystal. The entire time series was collected on one crystal to obtain the best difference maps between the light and dark states. See Graber et al.²³ for a more detailed description of the experimental setup and data collection geometry. The visible absorption spectrum of the crystal was taken after the X-ray data collection using the off-line BioCARS microspectrophotometer. The spectrum confirmed that the crystal consisted of a DHP-CO complex with no ferric DHP present.

Time-Resolved Data Processing. Laue data were processed using the programs Precognition/Epinorm²⁴ for scaling. All data sets were integrated to 1.8 Å, and data reduction statistics are summarized in Table S1 (Supporting Information). The reference dark-state DHP-CO structure (PDB 4JYQ) was refined against the room temperature dark Laue data set using the metaquo DHP structure (PDB 2QFK) as the starting model for the refinement in Refmac, CCP4.^{25,26} The final model of DHP-CO structure contained two identical protein molecules (chain A and chain B) in the asymmetric unit, which is the same dimeric form observed in the metaquo DHP structure. The final values of *R*_{cryst} and *R*_{free} were 15.9 and 21.2%, respectively. Refinement statistics are summarized in Table S2 (Supporting Information). Weighted time-dependent difference maps were calculated from weighted difference structure factor (SF) amplitudes $\Delta F_w = w(|F_{\text{DHP}^*}(t)| - |F_{\text{DHP-CO}}|)$ and phases derived from the reference DHP-CO structure. $|F_{\text{DHP-CO}}|$ is the dark-state SF amplitude and $|F_{\text{DHP}^*}(t)|$ is the corresponding time-dependent SF amplitude of the photoproduct at time *t*.²⁷ The weight, *w*, was calculated as²⁷

$$w = 1 / (1 + \Delta F^2 / \langle \Delta F \rangle^2 + \sigma_{\Delta F}^2 / \langle \sigma_{\Delta F} \rangle^2)$$

where $\Delta F = |F_{\text{DHP}^*}(t)| - |F_{\text{DHP-CO}}|$ is the difference of the structure factor amplitudes between time *t* and the dark state. $\sigma_{\Delta F}^2 = \sigma^2(F_{\text{DHP-CO}}) + \sigma^2(F_{\text{DHP}^*}(t))$ is the variance of ΔF and the sum of the variances of *F*_{DHP-CO} and *F*_{DHP*(*t)}. The symbol $\langle x \rangle$ denotes the mean value of all values of *x* in a data set.

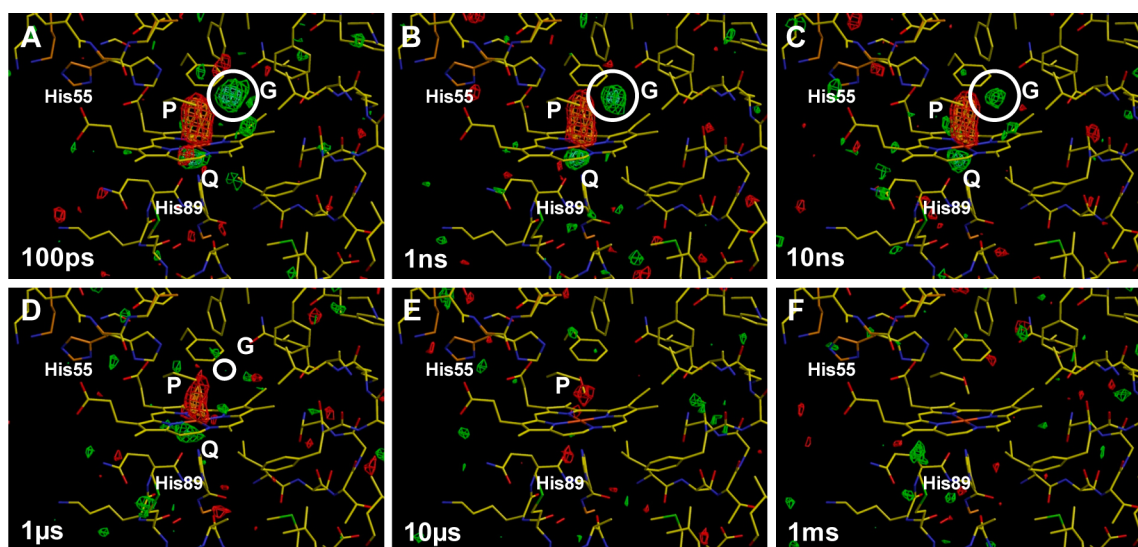


Figure 1. Weighted difference light–dark Fourier maps of the heme region (subunit A) of DHP-CO at different time delays after the laser pulse. The maps are calculated at 1.8 Å resolution as described in the Materials and Methods section. Light green and green signify positive difference electron densities, whereas orange and red signify negative densities. Two contouring levels are shown for both positive and negative densities: $\pm 3\sigma$ and $\pm 5\sigma$. The outer, darker colors (red and green) represent $\pm 3\sigma$ contours. The inner, lighter colors (orange and light green) represent $\pm 5\sigma$ contours (σ is the root-mean-square value of the difference density over the asymmetric unit). (A) 100 ps delay, (B) 1 ns delay, (C) 10 ns delay, (D) 1 μ s delay, (E) 10 μ s delay, and (F) 1 ms delay. The positive density in the circle, labeled G, shows the primary docking site of dissociated CO. Negative density P and positive density Q correspond to the loss of CO upon photolysis and the motion of Fe out of heme plane toward proximal histidine when CO dissociates, respectively.

Difference electron density maps for the heme region (subunit A) for different time delays, as displayed in XtalView,²⁸ are shown in Figure 1. Maps are contoured at $\pm 3\sigma$ and $\pm 5\sigma$, where σ is the root-mean-square value of the difference electron density across the asymmetric unit. Selected regions of the difference electron density maps were integrated by the program Promsk³ by summing up the density at grid points within a certain radius around a specific set of coordinates.⁵ A radius of 1.2 Å around C and O coordinates was used to determine the time dependence of the negative density at the CO binding site. In case of the positive density at the CO primary docking site (Xe1), a single sphere was used, centered at the density observed at 100 ps and with a larger radius of 1.4 Å. Integrated difference electron densities at the CO binding site and at the CO Xe1 site are shown in Figure 2.

Molecular Dynamics Simulation of Photolysis DHP-CO. The NAMD code²⁹ was used to study trajectories of photolyzed CO in DHP. The simulation parameters consisted of a time step of 2 fs, consistent with application of the Rattle algorithm,³⁰ a cutoff of 12 Å, and a switching distance of 1.5 Å. The DHP protein was surrounded by 9254 H₂O molecules in a box with dimensions 60 × 58 × 62 Å³. The particle-mesh Ewald approach was used to calculate electrostatic contributions to the potential.³¹ The force field used was the CHARMM27 force field. A monomer DHP protein taken originally from the 2QFK crystal structure³² was minimized and equilibrated for 1 ns. Subsequently, production dynamics were run for 20 ns. Both of the distal histidine (H55) tautomers (ϵ and δ) were studied in parallel simulations in otherwise identical systems.

RESULTS AND DISCUSSION

Observation of Photolyzed Ligand Trajectory and Rapid Recombination in DHP*CO. Short laser pulses (~35 ps) at 480 nm were used to photodissociate CO molecules, and the resulting DHP*CO photoproducts were probed by 100 ps

X-ray pulses at various time delays following the laser pulses (for experimental details, see the Materials and Methods). Difference Fourier maps corresponding to six time delays (100 ps, 1 ns, 10 ns, 1 μ s, 10 μ s, and 1 ms) (Figure 1A–F) reveal the differences between the average structure at a time delay t , DHP*CO(t), and the structure of the dark state, DHP-CO (PDB 4JYQ). An alternative view of Figure 1 with a white background is provided in the Supporting Information (Figure S1). Integration of the negative difference electron density at 100 ps at the CO-bound location (labeled P in Figure 1) indicates that ~11.3% of the CO is photodissociated (average value of subunits A and B shown in Figure 2). The magnitude of feature P decreases with time as photodissociated CO (CO) rebinds with a time constant on the order of magnitude $\tau \sim 1 \mu$ s (Figure 2). The positive features circled and labeled G in difference maps with time delays 100 ps (Figure 1A), 1 ns (Figure 1B), and 10 ns (Figure 1C) correspond to the CO

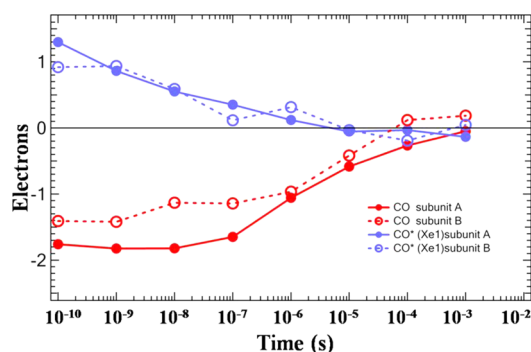


Figure 2. Time courses for integrated difference electron densities in weighted light–dark maps for subunits A and B of DHP. The red traces represent the CO heme Fe-binding site (site P), and the blue traces correspond to the CO in the Xe1-binding site (site G).

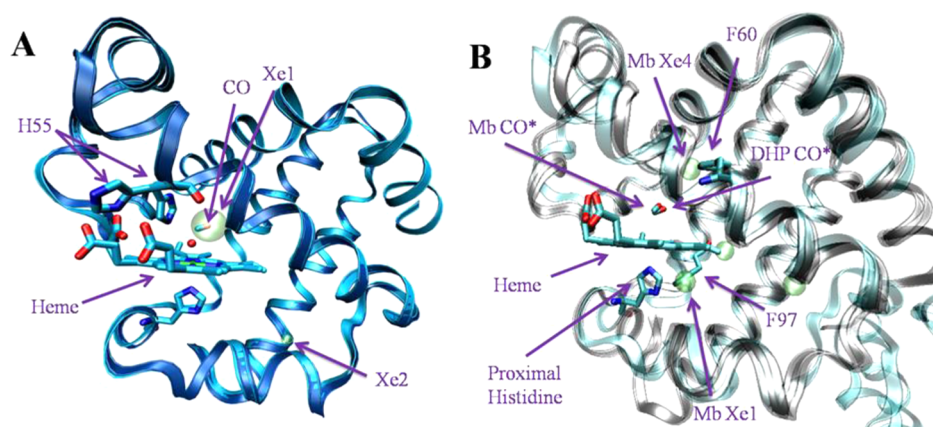


Figure 3. (A) Ribbon diagram of the overlaid metaquo structure of DHP derivatized with Xe (PDB 3MOU, cyan) and DHP-CO structure (blue). The two Xe-binding sites are occupancy-weighted in the figure (Xe1 = 0.4 and Xe2 = 0.1). The water molecule above heme Fe is present only in the metaquo DHP structure. The bound CO molecule in DHP-CO is not shown. Instead, a location of the CO molecule after photolysis is shown on the basis of the positive density at the Xe1-binding site in the 100 ps and 1 ns difference electron density maps (Figure 1). (B) Ribbon diagram of the overlaid structures of the DHP-CO (in cyan; the bound CO molecule is not shown, and the location of photodissociated CO is shown), SWMb*CO B site (PDB 2G0V, in gray), and SWMb derivatized with Xe (PDB 2W6W, in gray). The location of photodissociated CO is based on the location of positive CO density in the 100 ps and 1 ns difference maps. The location of photodissociated CO at site B in SWMb*CO (on the basis of the location of positive CO density in the 100 ps difference map) is also shown, indicating nearly the same initial location of the photodissociated CO in the two molecules. Green spheres indicate locations of four Xe cavities in SWMb.

located in the Xe1 docking site (a trace of this feature is also present at 1 μ s, Figure 1D). The coordinates for the photolyzed CO molecule are given in pdb format in the Supporting Information. Unlike SWMb, which has four Xe-binding sites, there is only one identifiable Xe-binding site inside DHP (Xe1).¹³ Although the result in Figure 1 may appear similar to the trajectories in SWMb*CO,^{2,3,34} there are major differences, which are related to the difference in function of DHP. The open distal pocket of DHP, which permits the binding of molecules as large as 2,4,6-tribromophenol (2,4,6-TBP), inside the globin³⁵ means that there is less hindrance to ligand escape but there is also less hindrance for ligand entry and binding to the heme Fe. One piece of evidence for this difference is the lag in the decrease of integrated negative density P relative to the decrease in positive density G at the Xe1 docking site (Figure 2), which suggests that CO has at least partially escaped from the protein on the time scale from 10 ns to 10 μ s. The observation of CO escape in the crystal is consistent with the fact that the geminate yield in DHP A is essentially zero in solution. At ambient temperature in aqueous solution, the yield for CO escape in DHP-CO is \sim 1 compared to 0.96 in SWMbCO.³³

Comparison of the CO Trajectory in DHP*CO and SWMb*CO. Figure 3A shows that the docking site of the CO coincides with the Xe-binding site Xe1 in DHP. Integration of difference electron density at docking site (Xe1) in the $\rho(\text{DHP*CO}) - \rho(\text{DHP-CO})$ difference map (average of subunit A and B) at 100 ps indicates that about 70% of CO is located in Xe1 (Figure 2). The remaining \sim 30% of CO at 100 ps could not be located above 3σ ; thus, further migration of CO beyond the Xe1 docking site could not be detected. These results indicate that DHP possesses a significantly different CO migration pathway than that observed in photolyzed SWMb*CO. In the first place, CO recombination with the heme Fe is completed \sim 10 times faster in DHP (\sim 10 μ s) than in wt Mb (\sim 100 μ s).^{1,34} The difference in the CO migration pathway in DHP*CO relative to SWMb*CO results from structural differences evident in the Xe crystal structures of the

respective proteins. To understand the differences, we can compare the Xe occupancies in the various sites of SWMb and DHP X-ray crystal structures in the presence of high-pressure Xe. There are four Xe binding sites observed in SWMb, with the Xe1 site close to fully occupied in the X-ray structure and sites Xe2–Xe4 occupied by Xe at 40–50%.³⁶ In DHP, only one internal Xe-binding site is present, occupied at \sim 40%, with a second site that has only \sim 10% occupation located on the surface of the protein.¹³ The DHP Xe1-binding site is above the heme and coincides with the CO density at 100 ps (Figure 3A). In contrast to DHP, the largest Xe-binding site in SWMb, Xe1, is on the proximal side of the heme.³⁶ Although in DHP photodissociated CO remains at the Xe1-binding site of DHP (Figure 3A), in SWMb, CO migrates from the primary distal docking site B to more remote cavities Xe4 to Xe1 in a temperature-dependent manner.^{2,3,34} To relate the migration of CO in the photolyzed X-ray crystal structures to the different functions of DHP and SWMb, we need to differentiate between the initially occupied docking site of SWMb and the protein cavities that are identified by Xe binding crystal structures.

We can distinguish between a cavity, which is identified by occupancy of a Xe atom in an X-ray crystal structure, and a docking site, which is a transiently formed volume that can accommodate a photolyzed CO ligand. In DHP*CO, the photolyzed CO ligand migrates directly to the Xe1-binding site, which is a permanent cavity in the protein. There appears to be no hindrance to ligand migration in the distal pocket of DHP. However, the primary CO docking site B in SWMb*CO is close to the location where a water molecule resides in the deoxy Mb distal pocket³⁴ and is not coincident with any of the SWMb Xe-binding sites. From the primary site, the CO molecule proceeds to the proximal Xe1 cavity, but this occurs on the 100 ns time scale.^{2,3,20,34} The access from the primary site to the permanent Xe-binding cavities can be increased by site-directed mutation.³⁷ The fact that CO is transiently trapped near the heme Fe in SWMb*CO suggests that the B site is occupied only because of the excess thermal energy of photolysis that permits the CO to displace amino acids in the

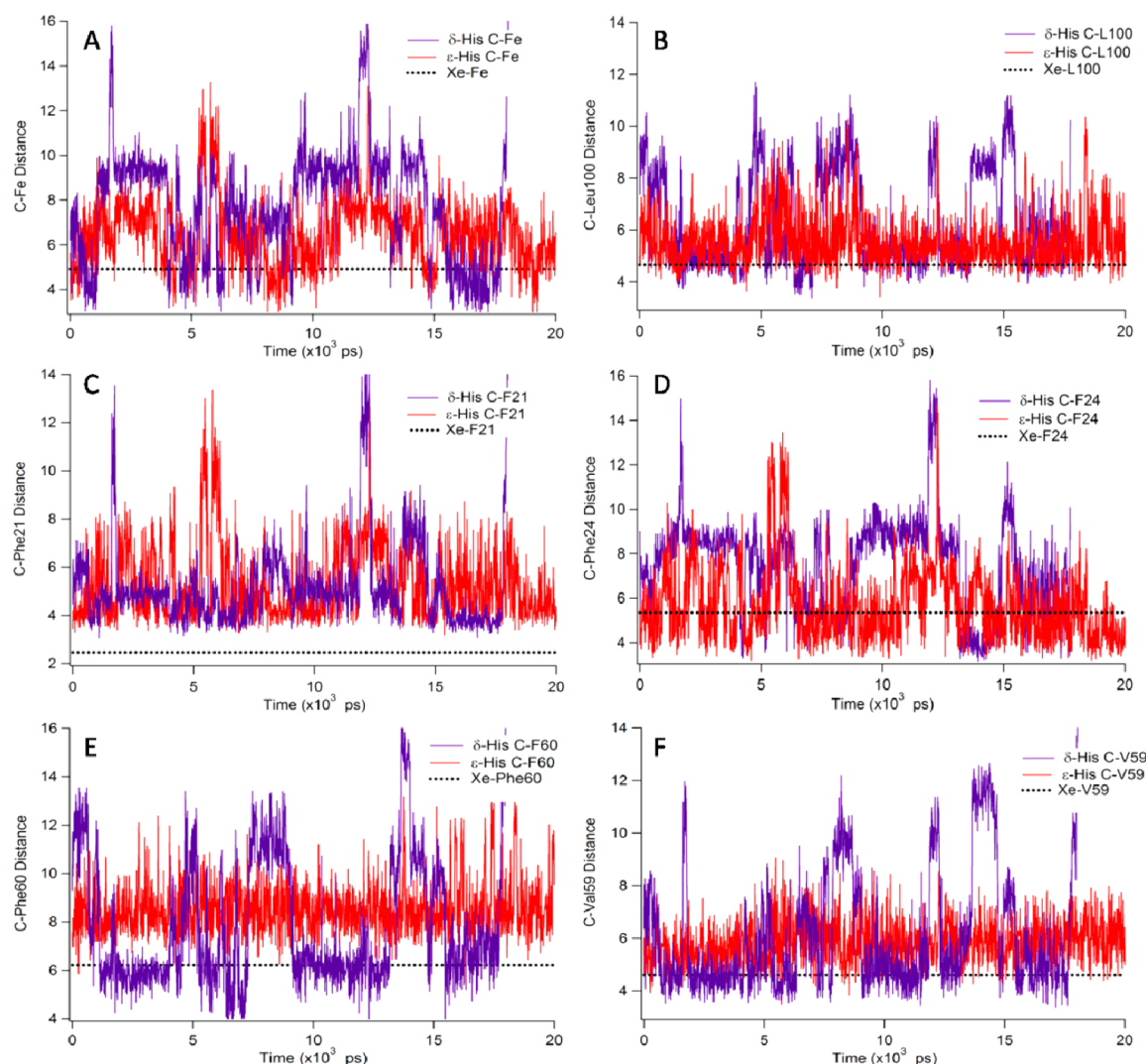


Figure 4. Distances (in Å) from the dissociated CO carbon atom to the heme Fe and key amino acid residues surrounding the Xe1-binding site as a function of time during MD simulations. (A) Distance from the CO carbon to the heme, (B) distance from the CO carbon to Leu100, (C) distance from the CO carbon to Phe21, (D) distance from the CO carbon to Phe24, (E) distance from the CO carbon to Phe60, and (F) distance from the CO carbon to Val59.

distal pocket. Residues Leu29 and Ile107 surrounding the B state are pushed away by photodissociated CO as CO moves to the B state at 100 ps, as evident from the room-temperature time-resolved X-ray data.² Moreover, in the rigid SWMb*CO structure at 40 K, CO is initially observed only ~1 Å from its bound location.³⁸ Only after an extended illumination over several hours was CO observed to gradually shift in the distal pocket to the B site observed in the room-temperature time-resolved experiments, about 2.5 Å away from the bound location.³⁹ However, this site is still not the same as the nearest Xe-binding site in SWMb (Xe4). These results suggest that there is a constrained distal docking site in Mb, which is absent in DHP. This difference is evident in the appearance of two CO absorption bands in the cryogenic FTIR spectrum of photolyzed SWMb*CO corresponding to the B₁ and B₂ states.⁴⁰ DHP*CO lacks this features and has one major band in the cryogenic photoproduct spectrum, suggesting that CO migrates to a relatively large protein cavity (Xe1) in DHP.³³ The behavior of SWMb*CO indicates gating of the ligand motion by the protein, consistent with the fact that SWMb*CO has a sufficiently constrained distal pocket that it

cannot accommodate both H₂O and O₂ (or CO) at the same time. Thus, the SWMb distal pocket acts as a valve that permits only one small molecule to transit at a time. DHP lacks this valve and permits CO to move more freely through the distal pocket as well as to escape much more readily than in SWMbCO.

Molecular Dynamics Simulation of DHP-CO. To examine the dynamics of the CO ligand trajectories, molecular dynamics (MD) simulations were conducted on photolyzed DHP*CO similar to simulations that have been carried out on SWMb*CO and HbI*CO.^{4,41–43} MD simulations were carried out for both the δ - and ϵ -tautomers of the distal histidine, His 55, with a free CO molecule that can migrate from a starting location above the heme Fe prior to equilibration. Figure 4 shows the distances from the CO carbon atom to the heme Fe and key amino acid residues surrounding the Xe1-binding site. During the simulation, the free CO molecule was observed to dwell in the Xe1-binding site for the majority of the simulation time. The distances from the Xe1-binding site in the DHP structure (PDB 3MOU)¹³ to the α -carbon of each of the surrounding amino acids are shown as dotted black lines in the

figure. The δ -His tautomer shows more variation in the CO position, which is divided between the Xe-binding site and a site in the distal pocket near the heme Fe. The CO ligand leaves the distal pocket after 18 and 20 ns in the δ -His and ϵ -His tautomer, respectively. Given the greater apparent fluctuation of the CO in the δ -tautomer of H55, it is not surprising that the CO escapes an earlier time in that simulation. However, CO escape is relatively rapid in both simulations, consistent with the hypothesis that DHP has a more open distal pocket than in other myoglobins and hemoglobins. The behavior is quite different from SWMb*CO in which CO is observed in the docking (or B) site and typical escape times are on the order of 100–200 ns⁴¹ (i.e., 10 times longer than both the measured³³ and simulated times for DHP*CO presented in Figure 4).

Figure 4A shows that, up to the point of CO ligand escape, the average Fe–C distance is 7.6 and 6.6 Å for the δ - and ϵ -tautomer of H55, respectively. Figure 4B shows the complementary aspect of the CO trajectory. Because L100 is in the back of the Xe1-binding cavity farthest from the heme Fe, the correlation of the distances in Figure 4A,B shows that CO fluctuates between a site near the Fe and the Xe1-binding site in the presence of the δ -tautomer. Although this close site in DHP*CO is similar in distance to the heme Fe to the B state in SWMb*CO, the behavior is quite different. The CO is not trapped near the Fe in DHP but rather visits that site as an excursion from the principal location, which is the DHP Xe1-binding site.

Function of Cavities in SWMb and HbI as a Protection against Autoxidation. The role of cavities in SWMb and HbI has been studied in terms of both dynamics and function.^{2,4,44,45} The primary function of both HbI and SWMb is oxygen transport and storage, which requires a Fe²⁺ state for the heme. Hemoglobins, and to a lesser extent myoglobins, in higher organisms are responsive to a large number of allosteric effectors, such as H⁺ (the Bohr effect), Cl[−], Ca²⁺, inositol hexaphosphate, and so on, which modulate the release of O₂.⁴⁶ Although the interior multiple cavities surrounding the heme in HbI and SWMb are not thought to be required for O₂ migration in and out of the protein, they may serve to permit O₂ to be sequestered for some time following release from the heme Fe (or in reverse when entering the protein to bind to the heme Fe).⁴⁷ Because the rate of autoxidation of oxyferrous SWMb is accelerated by H⁺, the hydrophobic interior cavities in SWMb may prevent the attack of H⁺ by sequestering O₂ from H₂O.⁴⁸ It is possible that O₂ passes through the cavities in response to transient entry of H₂O into the distal pocket. Because allosteric effects tune the binding constant, they may also affect the kinetics of migration inside the protein in a manner that is appropriate for the physiological role of the globin. The water entry into the distal pocket of Mb after photodissociated CO migrates into proximal site²² supports the hypothesis that Mb has a relatively small distal cavity, which serves to separate O₂ from H₂O molecules when O₂ is bound to the heme Fe. Thus, the amino acids in the distal cavity of SWMb act like a valve that controls the diatomic ligand trajectory and isolates it from H₂O, and particularly from H₃O⁺, to slow the autoxidation rate. The valve significantly impedes ligand diffusion by a second molecule into the distal pocket of SWMb. The autoxidation rate of SWMb increases if the distal pocket is opened by site-directed mutagenesis and conversely is slowed significantly for mutations that further occlude the distal pocket.⁴⁹

DHP lacks the multiple Xe-binding-site structure of SWMb and instead has only one internal Xe-binding cavity, Xe1.¹³ As shown in Figure 3B, the Xe1 and Xe4 sites in SWMb are blocked by Phe side chains (F97 and F60, respectively) in DHP. Therefore, DHP does not provide the extensive set of protein cavities observed in HbI and SWMb nor does DHP have the degree of steric constraint near the heme Fe atom seen SWMb and HbI. Therefore, photodissociated CO migrates into DHP Xe1 cavity without any hindrance. Moreover, CO can rapidly recombine from the Xe1 site, as shown in Figure 1. It is evident that the distal pocket of DHP is larger than that of SWMb because there are X-ray crystal structures and spectroscopy data that show that a range of 4-halophenols and 2,4,6-trihalophenols bind in the distal pocket of DHP.^{15,35,50} The studies of SWMb with relatively large isocyanates in the distal pocket represent a qualitatively different mode of binding because those molecules are all bound to the heme Fe.⁵¹ Crystallographic studies of isocyanide binding in Mb have provided information on entry/exit pathways for diatomic ligands.^{51,52} Although these are considered large molecules, the volume of the *n*-butyl group (the largest in the series) is still ~30% smaller than that of 2,4,6-TBP, which is the native substrate of DHP.

DHP is not susceptible to autoxidation because of its high Fe(III)/Fe(II) reduction potential.⁵³ In fact, DHP has a reduction potential of $E^{\circ} = +204$ mV, which is the highest of any monomeric hemoglobin or myoglobin studied to date.⁵³ The very high redox potential indicates that Fe(II) is favored over Fe(III) under physiological conditions. Consequently, DHP has such a low autoxidation rate that it appears not to require the same safeguards as SWMb to protect against protonation of bound O₂. For this reason, we hypothesize that SWMb and other similar globins require a valve that permits O₂ to bind and unbind without any contact with other small molecules. However, unlike these globins, DHP must have an open distal pocket, lacking the kind of small-molecule valve found in SWMb, because the DHP mechanism requires the initiation of catalysis by the displacement of bound O₂ by H₂O₂. Thus, both molecules must be simultaneously present in the distal pocket.¹⁶ Such a mechanism would be impossible in SWMb and other globins because the valve would only permit one of the two molecules into the distal pocket at any given time.

CONCLUSIONS

The time-resolved X-ray structural data presented in Figure 1 show that single Xe binding in DHP is correlated with the bifunctional property of DHP: oxygen storage and peroxidase activity. The distal cavity in DHP has an open structure, consistent with its capacity to bind both 4-BP and 2,4,6-TBP at different internal sites.³⁵ The distal Xe-binding site appears to play a key role in stabilizing the binding of 4-BP.¹³ Moreover, substrate binding at a different internal site has been observed to trigger the H₂O₂ displacement reaction at the heme Fe.¹⁶ The occupation of the Xe-binding site by CO observed in the time-resolved X-ray data suggests that this site could be transiently occupied by H₂O₂ prior to displacing the O₂ bound to the heme Fe. The fact that photolyzed CO occupies the Xe1-binding site and rapidly recombines with the heme Fe reveals how facile it would be for an H₂O₂ molecule to exchange with O₂ from this site. Once this has occurred, O₂ could escape into the solvent from the Xe1-binding site. Thus, time-resolved X-ray crystallography reveals important functional differences in

globins specialized for O₂ transport and storage and those that can have auxiliary functions in detoxification. Simple organisms such as *A. ornata* have no liver or other organ that specializes in detoxification and thus it appears that the dehaloperoxidase-hemoglobin is a multifunctional protein that has evolved to provide both O₂ transport and detoxification functions. The present study shows that time-resolved X-ray crystallography has tremendous potential for elucidating function based on characteristic differences in the photolyzed CO dynamics.

■ ASSOCIATED CONTENT

■ Supporting Information

Time-resolved X-ray crystallographic data reduction statistics, refinement statistics for the dark DHP-CO crystal structure, and an alternative view of Figure 1 with a white background. This material is available free of charge via the Internet at <http://pubs.acs.org>.

Accession Codes

Coordinates and structure factors have been deposited in the Protein Data Bank under accession no. 4JYQ.

■ AUTHOR INFORMATION

Corresponding Author

*E-mail: Stefan_Franzen@ncsu.edu. Phone: 919-515-8915.

Funding

We thank the Army Research Office for support through grant LS-57681. Use of the Advanced Photon Source was supported by the U.S. Department of Energy, Basic Energy Sciences, Office of Science, under contract no. DE-AC02-06CH11357. Use of the BioCARS Sector 14 was supported by the National Institutes of Health, National Institute of General Medical Sciences grant P41GM103543 (formerly National Center for Research Resources P41RR007707).

Notes

The authors declare no competing financial interest.

■ REFERENCES

- (1) Srajer, V.; Teng, T. Y.; Ursby, T.; Pradervand, C.; Ren, Z.; Adachi, S.; Schildkamp, W.; Bourgeois, D.; Wulff, M.; and Moffat, K. (1996) Photolysis of the carbon monoxide complex of myoglobin: Nano-second time-resolved crystallography. *Science* 274, 1726–1729.
- (2) Schotte, F.; Lim, M. H.; Jackson, T. A.; Smirnov, A. V.; Soman, J.; Olson, J. S.; Phillips, G. N.; Wulff, M.; and Anfinrud, P. A. (2003) Watching a protein as it functions with 150-ps time-resolved X-ray crystallography. *Science* 300, 1944–1947.
- (3) Schmidt, M.; Nienhaus, K.; Pahl, R.; Krasselt, A.; Anderson, S.; Parak, F.; Nienhaus, G. U.; and Srajer, V. (2005) Ligand migration pathway and protein dynamics in myoglobin: A time-resolved crystallographic study on L29W MbCO. *Proc. Natl. Acad. Sci. U.S.A.* 102, 11704–11709.
- (4) Knapp, J. E.; Pahl, R.; Cohen, J.; Nichols, J. C.; Schulten, K.; Gibson, Q. H.; Srajer, V.; and Royer, W. E. (2009) Ligand migration and cavities within scapharca dimeric Hbl: Studies by time-resolved crystallography, Xe binding, and computational analysis. *Structure* 17, 1494–1504.
- (5) Knapp, J. E.; Pahl, R.; Srajer, V.; and Royer, W. E. (2006) Allosteric action in real time: Time-resolved crystallographic studies of a cooperative dimeric hemoglobin. *Proc Natl Acad Sci U.S.A.* 103, 7649–7654.
- (6) Scott, E. E.; Gibson, Q. H.; and Olson, J. S. (2001) Mapping the pathways for O₂ entry into and exit from myoglobin. *J. Biol. Chem.* 276, 5177–5188.

- (7) Olson, J. S.; Soman, J.; and Phillips, G. N. (2007) Ligand pathways in myoglobin: A review of trp cavity mutations. *IUBMB Life* 59, 552–562.
- (8) Nienhaus, G. U., and Nienhaus, K. (2002) Infrared study of carbon monoxide migration among internal cavities of myoglobin mutant L29W. *J. Biol. Phys.* 28, 163–172.
- (9) Nienhaus, K.; Deng, P. C.; Kriegl, J. M.; and Nienhaus, G. U. (2003) Structural dynamics of myoglobin: Spectroscopic and structural characterization of ligand docking sites in myoglobin mutant L29W. *Biochemistry* 42, 9633–9646.
- (10) Nienhaus, K.; Ostermann, A.; Nienhaus, G. U.; Parak, F. G.; and Schmidt, M. (2005) Ligand migration and protein fluctuations in myoglobin mutant L29W. *Biochemistry* 44, 5095–5105.
- (11) Nienhaus, K.; Knapp, J. E.; Palladino, P.; Royer, W. E.; and Nienhaus, G. U. (2007) Ligand migration and binding in the dimeric hemoglobin of *Scapharca inaequivalvis*. *Biochemistry* 46, 14018–14031.
- (12) Steinbach, P. J.; Ansari, A.; Berendzen, J.; Braundstein, D.; Chu, K.; Cowen, B. R.; Ehrenstein, D.; Frauenfelder, H.; Johnson, J. B.; Lamb, D. C.; Luck, S.; Mourant, J. R.; Nienhaus, G. U.; Ormos, P.; Philipp, R.; Xie, A.; and Young, R. D. (1991) Ligand binding to heme proteins: Connection between dynamics and function. *Biochemistry* 30, 3988–4001.
- (13) de Serrano, V., and Franzen, S. (2012) Structural evidence for stabilization of inhibitor binding by a protein cavity in the dehaloperoxidase-hemoglobin from *Amphitrite ornata*. *Pept. Sci.* 98, 27–35.
- (14) Chen, Y. P.; Woodin, S. A.; Lincoln, D. E.; and Lovell, C. R. (1996) An unusual dehalogenating peroxidase from the marine terebellid polychaete *Amphitrite ornata*. *J. Biol. Chem.* 271, 4609–4612.
- (15) Thompson, M. K.; Ghiladi, R. A.; and Franzen, S. (2012) The dehaloperoxidase paradox. *Biochim. Biophys. Acta* 1842, 578–588.
- (16) D'Antonio, J., and Ghiladi, R. A. (2011) Reactivity of deoxy- and oxyferrous dehaloperoxidase B from *Amphitrite ornata*: Identification of compound II and its ferrous-hydroperoxide precursor. *Biochemistry* 50, 5999–6011.
- (17) Du, J.; Sono, M.; and Dawson, J. H. (2010) Functional switching of *Amphitrite ornata* dehaloperoxidase from O₂ binding globin to peroxidase enzyme facilitated by halophenol substrate and H₂O₂. *Biochemistry* 49, 6064–6069.
- (18) Dunford, B. H. (1999) *Heme Peroxidases*, John Wiley and Sons, New York.
- (19) Gumiero, A.; Murphy, E. J.; Metcalfe, C. L.; Moody, P. C. E.; and Raven, E. L. (2010) An analysis of substrate binding interactions in the heme peroxidase enzymes: A structural perspective. *Arch. Biochem. Biophys.* 500, 13–20.
- (20) Schotte, F.; Soman, J.; Olson, J. S.; Wulff, M.; and Anfinrud, P. A. (2004) Picosecond time-resolved X-ray crystallography: Probing protein function in real time. *J. Struct. Biol.* 147, 235–246.
- (21) Cao, W. X.; Christian, J. F.; Champion, P. M.; Rosca, F.; and Sage, J. T. (2001) Water penetration and binding to ferric myoglobin. *Biochemistry* 40, 5728–5737.
- (22) Goldbeck, R. A.; Bhaskaran, S.; Ortega, C.; Mendoza, J. L.; Olson, J. S.; Soman, J.; Kliger, D. S.; and Esquerra, R. M. (2006) Water and ligand entry in myoglobin: Assessing the speed and extent of heme pocket hydration after CO photodissociation. *Proc. Natl. Acad. Sci. U.S.A.* 103, 1254–1259.
- (23) Graber, T.; Anderson, S.; Brewer, H.; Chen, Y. S.; Cho, H. S.; Dashdorj, N.; Henning, R. W.; Kosheleva, I.; Macha, G.; Meron, M.; Pahl, R.; Ren, Z.; Ruan, S.; Schotte, F.; Rajer, V. S.; Viccaro, P. J.; Westferro, F.; Anfinrud, P.; and Moffat, K. (2011) BioCARS: a synchrotron resource for time-resolved X-ray science. *J. Synchrotron Radiat.* 18, 658–670.
- (24) Ren, Z. (2010) *Precognition User Guide*, RenZ Research Inc., Westmont, IL.
- (25) Krissinel, E. B.; Winn, M. D.; Ballard, C. C.; Ashton, A. W.; Patel, P.; Potterton, E. A.; McNicholas, S. J.; Cowtan, K. D.; and Emsley, P. (2004) The new CCP4 coordinate library as a toolkit for the design of

coordinate-related applications in protein crystallography. *Acta Crystallogr., Sect. D* 60, 2250–2255.

(26) Potterton, L., McNicholas, S., Krissinel, E., Gruber, J., Cowtan, K., Emsley, P., Murshudov, G. N., Cohen, S., Perrakis, A., and Noble, M. (2004) Developments in the CCP4 molecular-graphics project. *Acta Crystallogr., Sect. D* 60, 2288–2294.

(27) Ren, Z., Perman, B., Srajer, V., Teng, T. Y., Pradervand, C., Bourgeois, D., Schotte, F., Ursby, T., Kort, R., Wulff, M., and Moffat, K. (2001) A molecular movie at 1.8 angstrom resolution displays the photocycle of photoactive yellow protein, a eubacterial blue-light receptor, from nanoseconds to seconds. *Biochemistry* 40, 13788–13801.

(28) McRee, D. (1993) *Practical Protein Crystallography*, Academic Press, San Diego, CA.

(29) Phillips, J. C., Braun, R., Wang, W., Gumbart, J., Tajkhorshid, E., Villa, E., Chipot, C., Skeel, R. D., Kale, L., and Schulten, K. (2005) Scalable molecular dynamics with NAMD. *J. Comput. Chem.* 26, 1781–1802.

(30) Andersen, H. C. (1983) Rattle: A “velocity” version of the shake algorithm for molecular dynamics calculations. *J. Comput. Phys.* 52, 24–34.

(31) Sagui, C., and Darden, T. (2001) Multigrid methods for classical molecular dynamics simulations of biomolecules. *J. Chem. Phys.* 114, 6578–6591.

(32) de Serrano, V., Chen, Z. X., Davis, M. F., and Franzen, S. (2007) X-ray crystal structural analysis of the binding site in the ferric and oxyferric forms of the recombinant heme dehaloperoxidase cloned from *Amphitrite ornata*. *Acta Crystallogr., Sect. D* 63, 1094–1101.

(33) Nienhaus, K., Deng, P., Belyea, J., Franzen, S., and Nienhaus, G. U. (2006) Spectroscopic study of substrate binding to the carbon-monooxy form of dehaloperoxidase from *Amphitrite ornata*. *J. Phys. Chem. B* 110, 13264–13276.

(34) Srajer, V., Ren, Z., Teng, T. Y., Schmidt, M., Ursby, T., Bourgeois, D., Pradervand, C., Schildkamp, W., Wulff, M., and Moffat, K. (2001) Protein conformational relaxation and ligand migration in myoglobin: A nanosecond to millisecond molecular movie from time-resolved Laue X-ray diffraction. *Biochemistry* 40, 13802–13815.

(35) Zhao, J., de Serrano, V., Zhao, J., Le, P., and Franzen, S. (2013) Structural and kinetic study of an internal substrate binding site in dehaloperoxidase-hemoglobin A from *Amphitrite ornata*. *Biochemistry* 52, 2427–2439.

(36) Tilton, R. F., Jr., Kuntz, I. D., Jr., and Petsko, G. A. (1984) Cavities in proteins: Structure of a metmyoglobin xenon complex solved to 1.9 Å. *Biochemistry* 23, 2849–2857.

(37) Brunori, M., Vallone, B., Cutruzzola, F., Travaglini-Allocatelli, C., Berendzen, J., Chu, K., Sweet, R. M., and Schlichting, I. (2000) The role of cavities in protein dynamics: Crystal structure of a photolytic intermediate of a mutant myoglobin. *Proc. Natl. Acad. Sci. U.S.A.* 97, 2058–2063.

(38) Teng, T.-Y., Srajer, V., and Moffat, K. (1994) Photolysis-induced structural changes in single crystals of carbonmonooxy myoglobin at 40 K. *Nat. Struct. Biol.* 1, 701–705.

(39) Teng, T. Y., Srajer, V., and Moffat, K. (1997) Initial trajectory of carbon monoxide after photodissociation from myoglobin at cryogenic temperatures. *Biochemistry* 36, 12087–12100.

(40) Lim, M. H., Jackson, T. A., and Anfinsen, P. A. (1997) Ultrafast rotation and trapping of carbon monoxide dissociated from myoglobin. *Nat. Struct. Biol.* 4, 209–214.

(41) Meller, J., and Elber, R. (1998) Computer simulations of carbon monoxide photodissociation in myoglobin: Structural interpretation of the B states. *Biophys. J.* 74, 789–802.

(42) Elber, R. (2010) Ligand diffusion in globins: simulations versus experiment. *Curr. Opin. Struct. Biol.* 20, 162–167.

(43) Ruscio, J. Z., Kumar, D., Shukla, M., Prisant, M. G., Murali, T. M., and Onufriev, A. V. (2008) Atomic level computational identification of ligand migration pathways between solvent and binding site in myoglobin. *Proc. Natl. Acad. Sci. U.S.A.* 105, 9204–9209.

(44) Frauenfelder, H., McMahon, B. H., Austin, R. H., Chu, K., and Groves, J. T. (2001) The role of structure, energy landscape, dynamics, and allostery in the enzymatic function of myoglobin. *Proc. Natl. Acad. Sci. U.S.A.* 98, 2370–2374.

(45) Beece, D., Eisenstein, L., Frauenfelder, H., Good, D., Marden, M. C., Reinisch, L., Reynolds, A. H., Sorensen, L. B., and Yue, K. T. (1980) Solvent viscosity and protein dynamics. *Biochemistry* 19, 5147–5157.

(46) Perutz, M. F., Wilkinson, A. J., Paoli, M., and Dodson, G. G. (1998) The stereochemical mechanism of the cooperative effects in hemoglobin revisited. *Annu. Rev. Biophys. Biomol. Struct.* 27, 1–34.

(47) Cohen, J., and Schulten, K. (2007) O₂ migration pathways are not conserved across proteins of a similar fold. *Biophys. J.* 93, 3591–3600.

(48) Brantley, R. E., Smerdon, S. J., Wilkinson, A. J., Singleton, E. W., and Olson, J. S. (1993) The mechanism of autooxidation in myoglobin. *J. Biol. Chem.* 268, 6995–7010.

(49) Carver, T. E., Brantley, R. E., Jr., Singleton, E. W., Arduini, R. M., Quillin, M. L., Phillips, G. N., Jr., and Olson, J. S. (1992) A novel site-directed mutant of myoglobin with an unusually high O₂ affinity and low autooxidation rate. *J. Biol. Chem.* 267, 14443–14450.

(50) Nienhaus, K., Nickel, E., Davis, M. F., Franzen, S., and Nienhaus, G. U. (2008) Determinants of substrate internalization in the distal pocket of dehaloperoxidase hemoglobin of *Amphitrite ornata*. *Biochemistry* 47, 12985–12994.

(51) Johnson, K. A., Olson, J. S., and Phillips, G. N., Jr. (1989) Structure of myoglobin-ethyl isocyanide histidine as a swinging door for ligand entry. *J. Mol. Biol.* 207, 459–463.

(52) Smith, R. D., Blouin, G. C., Johnson, K. A., Phillips, G. N., and Olson, J. S. (2010) Straight-chain alkyl isocyanides open the distal histidine gate in crystal structures of myoglobin. *Biochemistry* 49, 4977–4986.

(53) D’Antonio, E. L., Bowden, E. F., and Franzen, S. (2012) Thin-layer spectroelectrochemistry of the Fe(III)/Fe(II) redox reaction of dehaloperoxidase-hemoglobin. *J. Electroanal. Chem.* 668, 37–43.